# Viscoelastic Properties of Ionic Polymer Composites Reinforced by Soy Protein Isolate

**L. JONG**

National Center for Agricultural Utilization Research, Department of Agriculture, Agricultural Research Service, Illinois 61604

*Received 28 March 2005; revised 16 June 2005; accepted 4 August 2005*
*DOI: 10.1002/polb.20608*
*Published online in Wiley InterScience (www.interscience.wiley.com).*

**ABSTRACT:** Both linear and nonlinear viscoelastic properties of ionic polymer composites reinforced by soy protein isolate (SPI) were studied. Viscoelastic properties were related to the aggregate structure of fillers. The aggregate structure of SPI is consisted of submicron size of globule protein particles that form an open aggregate structure. SPI and carbon black (CB) aggregates characterized by scanning electron microscope and particle size analyzer indicate that CB aggregates have a smaller primary particle and aggregate size than SPI aggregates, but the SPI composites have a slightly greater elastic modulus in the linear viscoelastic region than the CB composites. The composite containing 3–40 wt % of SPI has a transition in the shear elastic modulus between 6 and 8 vol % filler, indicating a percolation threshold. CB composites also showed a modulus transition at <6 vol %. The change of fractional free volume with filler concentration as estimated from WLF fit of frequency shift factor also supports the existence of a percolation threshold. Nonlinear viscoelastic properties of filler, matrix, and composites suggested that the filler-immobilized rubber network generated a G′ maximum in the modulus-strain curves and the SPI formed a stronger filler network than the CB in these composites. © 2005 Wiley Periodicals, Inc.* J Polym Sci Part B: Polym Phys 43: 3503–3518, 2005

**Keywords:** composites; elastomers; proteins; soy; viscoelastic properties

## INTRODUCTION

The modulus of rubbers can be enhanced by natural materials, for example, oil palm wood,[1] crab shell chitin,[2] and bamboo fiber.[3] As a renewable material beneficial to our environment, soybean protein has been investigated as a component in plastic and adhesive applications,[4–7] but has been rarely investigated as a reinforcement component in elastomers. The attempt to use protein in rubber latex can be traced back to 1930s. A few patents had claimed the use of protein in rubber composites.[8–10] For example, an approximately fourfold increase in the rubber modulus had been demonstrated by the use of casein, a milk protein, in natural rubber latex.[10]

Structurally, soy protein isolate (SPI) is a globule protein and its aggregate is similar to particle aggregates. Dry SPI is a rigid material and has a shear elastic modulus of ~2 GPa under ambient conditions.[5] Because the high rigidity in reinforcement phase is one of the requirements in rubber reinforcement, dry SPI aggregates generated a significant reinforcement

Disclaimer: Names are necessary to factually report on available data; however, the USDA neither guarantees nor warrants the standard of the product, and the use of the name by USDA implies no approval of the product to the exclusion of others that may also be suitable.

*Correspondence to:* L. Jong (E-mail: jongl@ncaur.usda.gov)

Journal of Polymer Science: Part B: Polymer Physics, Vol. 43, 3503–3518 (2005)

effect in rubbers. Compared with carbon black (CB), SPI has both larger primary particle size and aggregate size. Despite micron size aggregates, dry soy protein gave a higher reinforcement effect than carbon black in rubbers at the same volume or weight fraction. The important factors involved in the rubber reinforcement are aggregate structure, effective filler volume fraction, filler–rubber interaction, and elastic modulus of filler clusters. Theoretical developments on the reinforcement mechanism of particle aggregates can be found in a recent review.[11] One of the theories on the particle-reinforced elastomer is cluster–cluster aggregation model (CCA) that relates the fractal structure of particle aggregate to the dynamic elastic modulus.[11,12] This model can describe the reinforcement mechanism above percolation threshold. The model description on the reinforcement effect of some carbon black and polymeric fillers has been shown to be reasonable.[11,13,14]

The objective of this study is to investigate the structure of soy protein aggregates and its effect in the rubber reinforcement, as well as the frequency dependent properties in both linear and nonlinear viscoelastic regions of these rubber composites. Carbon black with much smaller size is also used as a comparison to further the understanding of SPI composites. In this study, the rubber matrix chosen is a styrene–butadiene (SB) rubber containing a small amount of carboxylic acid containing monomer units. The rubber matrix does not require crosslinking reactions to achieve a network structure because the ionic functional groups can aggregate as crosslinking points. The presence of ionic groups can also interact with soy protein to provide some filler–rubber interactions. Soy protein contains a significant amount of carboxylic acid and substituted amine group.[15] The ionic interaction between protein and matrix is therefore possible. For practical applications, the issue of moisture sensitivity in some applications is always associated with natural materials, but it may be improved through product formulation or selective applications. For example, it may be used as an ingredient in multilayered structures, in coated objects, in high temperature applications, or in rubber parts functioning in greasy/oily environments where the moisture effect is minimum.

The rubber composites investigated here is prepared by casting films from the dispersion of soy protein and carboxylated styrene–butadiene latex. Carboxylated SB rubber is classified as an ion-containing polymer. Its viscoelastic properties are affected by molecular weight, degree of crosslinking, glass transition temperature ($T_g$), copolymer composition, the number of ionic functional groups, the size of ionic aggregation, the degree of neutralization, and the size of the neutralizing ions.[16,17] Previous studies also have shown honeycomb-like structures in the film of carboxylated latexes due to a higher concentration of carboxylic acid groups on the particle surface.[18] Mechanically, the elastic modulus of base rubber is not significant when compared with the modulus of filler network in highly filled elastomeric composites.[19]

## EXPERIMENTAL

### Materials

The SPI used in this research is a slightly enzyme hydrolyzed soy protein isolate (PROFAM 781, Archer Daniels Midland Company, Decatur, IL). It contains more than 90% protein, ~6% ash, and ~4% fat. Sodium hydroxide, used to adjust pH, is ACS grade. The carboxylated styrene–butadiene latex is a random copolymer of styrene, butadiene, and a small amount of carboxylic acid containing monomers (CP 620NA, Dow Chemical Company, Midland, MI). The glass transition temperature of SB Latex is ~10 °C, determined by differential scanning calorimetry (DSC). Styrene/butadiene ratio estimated from the glass transition temperatures of a series of commercially available SB is ~65/35. The dried latex is not known to be soluble in any solvent or a combination of solvents. The latex received has ~50% solids and a pH ~ 6. The particle size of latex is ~0.18 $\mu$m.

### Preparation of Composites

SPI was first dispersed in water and the pH was adjusted to 9 with sodium hydroxide. The alkaline SPI dispersion was then cooked under stirring at 55 °C for 60 min to help with the dispersion of SPI. After cooking, the cloudy SPI dispersion was then mixed homogeneously with alkaline SB latex and the pH of mixture was adjusted to 9. The final aqueous dispersion has 25% solids and 75% water. The composite of SPI and SB latex was prepared by first casting an emulsion of the blend onto an aluminum mold

covered with Teflon released sheet (BYTAC from Saint–Gobain Performance Plastics) and then allowing it to dry at 75 °C for 72 h. After drying at low temperature, the samples were removed from the mold and annealed at 110 and 140 °C for 24 h respectively. Dry composites containing 3–40% by weight of SPI were prepared. The film of 100% SB was prepared by adjusting the pH of latex to 9 and dried under the same conditions as that of the SPI/SB composites. Carbon black (CB) composites were prepared in the same way as that of protein by mixing an aqueous dispersion of carbon black and SB latex. A different batch of the same SB latex was used to prepare CB composites. Batch-to-batch variation of SB latex is small and has no effect on the results because the SB modulus is not significant when compared with the composite modulus. Aqueous dispersion of carbon black N-339 (Sid Richardson Carbon Co.) was prepared by dispersing carbon black in water with the aid of a surfactant, sodium lignosulfonate (Vanisperse CB, Lignotech USA, Rothschild, WI). The weight fraction of surfactant based on carbon black is 3%. The dispersion was homogenized at 10,000 rpm for 1 h. The dried SB film contains <0.3% moisture and the dried SPI/SB and CB/SB composites have moisture contents <0.8% as measured by halogen moisture analyzer (Mettler Toledo HR73) at 105 °C for 60 min. The weight fractions of soy protein in the composites were converted to volume fractions by measuring the density of SPI and composites, using a low viscosity poly(dimethylsiloxane) as an immersion liquid. For compression-molded samples, an aqueous mixture was first freeze-dried and then compression molded at 47 MPa and 140 °C for 2 h. After compression molding, the sample was relaxed at 140 °C for 24 h.

### Particle Size and Scattering Intensity

The particle size and size distribution of soy protein dispersion and SB latex were measured by a Horiba LA-930 laser scattering particle size analyzer, with the red light wavelength of 632.8 nm and the blue light wavelength of 405 nm. The measurement is based on Mie scattering theory and has a measurement range of 0.02–2000 $\mu$m. The accuracy of the instrument was verified with NIST traceable spherical polystyrene latex standards to be within ±2%. The average scattering curve was obtained from the 20 scans of a circulating dilute dispersion. Tumbling particles are assumed to be spheres. The method generates a volume or mass moment mean diameter (De Brouckere mean diameter). The $R_g$ of particles can be estimated from the volume or mass equivalent spheres using the relation $R_g = (3/5)^{1/2} R$, where $R$ is the radius of sphere. The volume weighted mean diameter for protein aggregates without sonication was 3.74 $\mu$m. The $R_g$ estimated from the equivalent sphere is ~1.45 $\mu$m and $qR_g$ is >1 in the limited $q$ range ($q$ = 0.0023–0.0032 $nm^{-1}$) at the end of the scattering curve. Volume weighted mean diameter of 0.18 $\mu$m was obtained for the spherical styrene–butadiene latex[18] and was in good agreement with particle size value of 0.18 $\mu$m supplied by Dow Chemical Company. The change of aggregate size was studied by a build-in 30 W 22.5 kHz ultrasonic probe. Scattering intensity versus scattering angle was also obtained from the same instrument to monitor the structure change of protein aggregates.

### Scanning Electron Microscopy

The morphology of the composites and soy protein aggregates were obtained by scanning electron microscopy (SEM) using JEOL JSM-6400V instrument. Images of these soy products were obtained by casting onto an aluminum substrate a dilute dispersion of soy protein at pH 9 and at a concentration of 0.004%. The samples on aluminum stubs were then coated with Au–Pd and examined under vacuum at ambient temperature.

### Dynamic Mechanical Measurements

For the frequency and time sweep experiments, the oscillatory shear storage and loss moduli, $G'(\omega)$and $G''(\omega)$, were measured using a Rheometric ARES-LSM rheometer equipped with a torsional rectangular geometry. Rectangular samples with a dimension of ~12.5 × 40 × 3 $mm^3$ were inserted between the top and bottom grips. The gap between the fixtures is ~20 mm. To obtain the frequency spectra of composites, the time–temperature superposition experiments were conducted with a reference temperature of 10 °C. The frequency range was from 0.1 to 100 rad/s and the temperature range was from 10 to 100 °C. The frequency master curve was obtained using RSI Orchestrator V6.5.8 software.

Temperature ramp experiments were conducted using torsion rectangular geometry, with

a heating rate of 1 °C/min and a temperature range from −40 °C to 140 °C. The soak time at each temperature after ramp was 15 s and the measurement duration at each temperature was 30 s. The sample dimensions were similar to that in the frequency and time-sweep experiments. The dynamic mechanical measurements were conducted at a frequency of 0.16 Hz (1 rad/s) and a strain of 0.05%.

The elastic modulus at linear region was obtained by a time-sweep experiment at 140 °C, 0.16 Hz (1 rad/s), and 0.05% strain. From the previous annealing experiments, it is known that the annealing in oven is completed in 24 h at 140 °C. However, all annealed samples were checked by the time-sweep experiments for 30–60 min and the average value at equilibrium (<1% increase in 30 min) was taken as the elastic modulus. Three to seven specimens were measured for each composite composition.

For all strain sweep-experiments, the oscillatory storage and loss moduli, $G'(\omega)$and $G''(\omega)$, were measured using a Rheometric ARES-LSM rheometer with a torsional rectangular geometry. The shear strain-controlled rheometer is capable of measuring the oscillatory strain down to $3 \times 10^{-5}$% strain (TA Instruments, Piscataway, NJ). The rheometer was calibrated in terms of torque, normal force, phase angle, and strain using the instrument procedure. A rectangular sample with dimension of ~12.5 × 20 × 3 $mm^3$ was inserted between the top and bottom grips. The gap between the fixtures was 5–6 mm to achieve a strain of ~15%. A sample length shorter than 5 mm is not desirable because of the shape change from the clamping at both ends of the sample. The frequency used in the measurements was 1 or 15 Hz. The oscillatory storage and loss moduli were measured over a strain range of ~0.001–15%. The actual strain sweep range was limited by sample geometry and motor compliance at large strain and transducer sensitivity at small strain. The data that was out of transducer range was rejected. Although harmonics in the displacement signal may be expected in nonlinear material, a previous study[20] indicated that the harmonics are not significant if the shearing does not exceed 100%. Each sample was conditioned at 80 or 140 °C for 30 min and then subjected to 8 cycles of dynamic strain sweep to study the stress softening effect. The delay between strain cycles is 100 s. For clarity, only data from the first, fourth, and eighth cycle are shown in the figures. To measure the recovery curves, the samples were allowed to recover at 140 °C for 24 h before the measurements.

## RESULTS AND DISCUSSION

### Aggregate Structure of Soy Protein

To understand the reinforcement of SPI filler, the structure of SPI aggregates was first characterized by SEM. The images of an SPI aggregate, a fractured SB, and a fractured SPI/SB composite containing 40% protein are shown in Figure 1. From Figure 1(a), it is observed that SPI aggregates are formed from submicron particles. The aggregates were observed even when it is cast from a dilute dispersion with a concentration of only 0.004%. The image of SB matrix shows a smooth surface and some fractured marks [Fig. 1(b)]. Compared with SB, the fractured surface of 40/60 SPI/SB composite shows homogeneously distributed SPI aggregates [Fig. 1(c)]. From the image analysis of 115 particles, the primary particle size of the aggregate has an average Feret diameter of 0.33 μm and a standard deviation of 14%, indicating that the distribution of primary particle size is not monodisperse. To characterize the size and size distribution of SPI aggregates in wet state, a particle size analyzer based on the principle of light scattering in dilute dispersion was used. The dry size can be related to wet size by SPI swelling ratio at pH 9. The swelling ratio was determined to be ~1.5 based on the protein swelling at equilibrium in SPI/SB composite containing 40% SPI. The result of wet size measurement is shown in Figure 2(a). The number average size of wet SPI aggregates is about 2.2 μm. The dry size of SPI aggregates is estimated to be ~1.5 μm by correcting the swelling effect. After it was sonicated for 1 h, the whole size distribu-

**Figure 1.** (a) SPI aggregates on a gray mottled aluminum substrate. The scale bar shown is 1 μm. (b) Liquid nitrogen fractured surface of SB without soy protein aggregates. The scale bar shown is 10 μm. (c) Liquid nitrogen fractured surface of a SPI/SB composite containing 40% SPI aggregates. The scale bar shown is 10 μm.

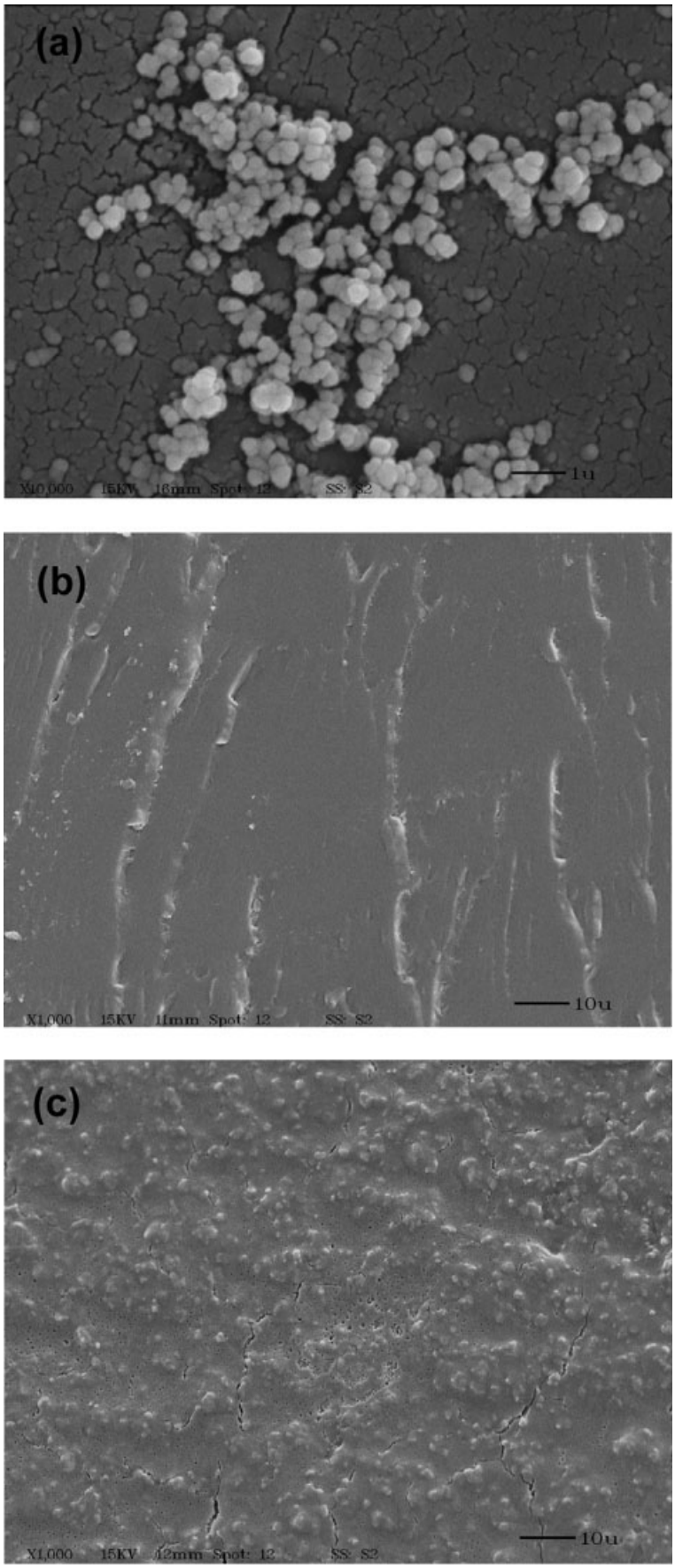
(a)
1u
(b)
X1,000 15KV 11mm Spot: 12 SS: S2
10u
(c)
X1,000 15KV 12mm Spot: 12 SS: S2
10u

**Figure 1.**

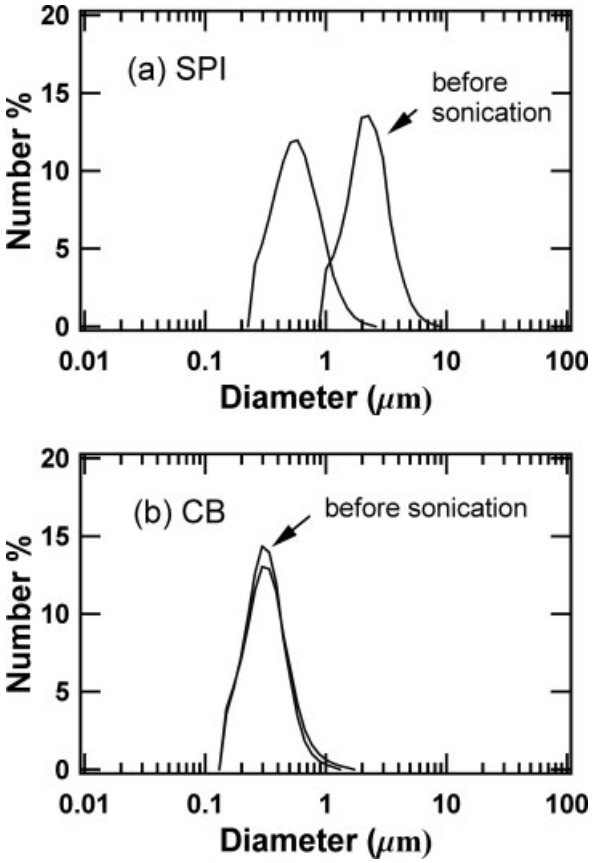


**Figure 2.** The number distribution of aggregate size in (a) SPI dispersion (b) Carbon black dispersion. One curve as indicated is before the sonication and the other is after the sonication treatment.

tion curve was shifted to the smaller size region and the average wet size was reduced to about 0.6 $\mu$m [Fig. 2(a)] or an equivalent dry size of $\sim$0.4 $\mu$m. Carbon black aggregates, however, have a primary particle size of $\sim$0.04 $\mu$m[21] and a number average size of $\sim$0.3 $\mu$m. The CB aggregates was not affected by the sonication or swelling. This indicates that carbon black aggregates are less likely to change during mixing, film casting, and heating. The dispersion of CB aggregates in SB matrix is shown in Figure 3. The micrographs showed a homogeneous distribution of CB aggregates in the fractured surface of a 30 wt % CB composite.

The aggregate structure of soy protein is similar to that of colloidal aggregates. The difference between soy protein aggregate and colloidal aggregate is that soy protein aggregate is already formed in soybean and the dispersion of protein is a de-aggregation process. Whereas, the formation of colloidal aggregates is a growth process where individual particles are forced to flocculate by the changing of conditions such as concentration, temperature, addition of salt, and pH. The determination of aggregate structure has been extensively investigated on colloidal aggregates, especially by computer simulation.[22,23] For diffusion limited cluster aggregates (DLCA), the fractal dimension of aggregates ($D_f$) is around 1.7–1.8. However, the fractal dimension in real systems can range from 1 to 3. A few methods have been used to determine the fractal dimension of aggregates, such as light scattering,[24–26] rheological measurement,[12] and image analysis.[27,28] For light scattering method, in the fractal region of scattering curve ($qR_g \gg 1$), $I(q)$ is proportional to $q^{-D_f}$, where $R_g$ is the radius of gyration and $q$ is the scattering vector.[24–26] To understand the stability of SPI aggregates, the dilute SPI dispersion was subjected to sonication. For soy protein aggregates, it was found that the degree of aggregation changed with the presence of SB latex and the time of sonication. The data in the limited $q$ range ($q$ = 0.0023–0.0032 nm$^{-1}$) at the end of each scattering curve can be fitted to a linear line with $R^2 \gg 0.999$. As shown in Figure 4(c), the slopes in this limited $q$ range decreased as the time of sonication increased. However, the slope can only be estimated as $D_f$ for aggregate size greater than $\sim$1.2 $\mu$m because the $qR_g$ is no longer $>$1 for smaller aggregates. This excludes the interpretation of the slope as $D_f$ for the sonication time longer than 45 min in Figure 4(a) and 8 min in Figure 4(b). Despite the limitation in the interpretation of slope using fractal theory, the trend in Figure 4(c) is consistent with Figure 2(a) and indicates the break-down of aggregate structure to simpler and smaller aggregates. Combined with the results from Figure 1(a) and Figure 2(a), it is likely that protein aggregate structure after sonication is only a simple aggregate of a few protein globules. With the presence of SB latex, the breakdown of SPI aggregates was accelerated; possibly, because of the surfactant effect of SB latex. This also indicates the protein aggregate structure can change during the mixing, heating, and film casting. In addition, it indicates an uncertainty as to whether or not the aggregate structure measured in the dilute dispersion is the same as that in the solid composites.

### Protein Network

The reinforcement effect of soy protein isolate (SPI) in carboxylated styrene–butadiene rubber

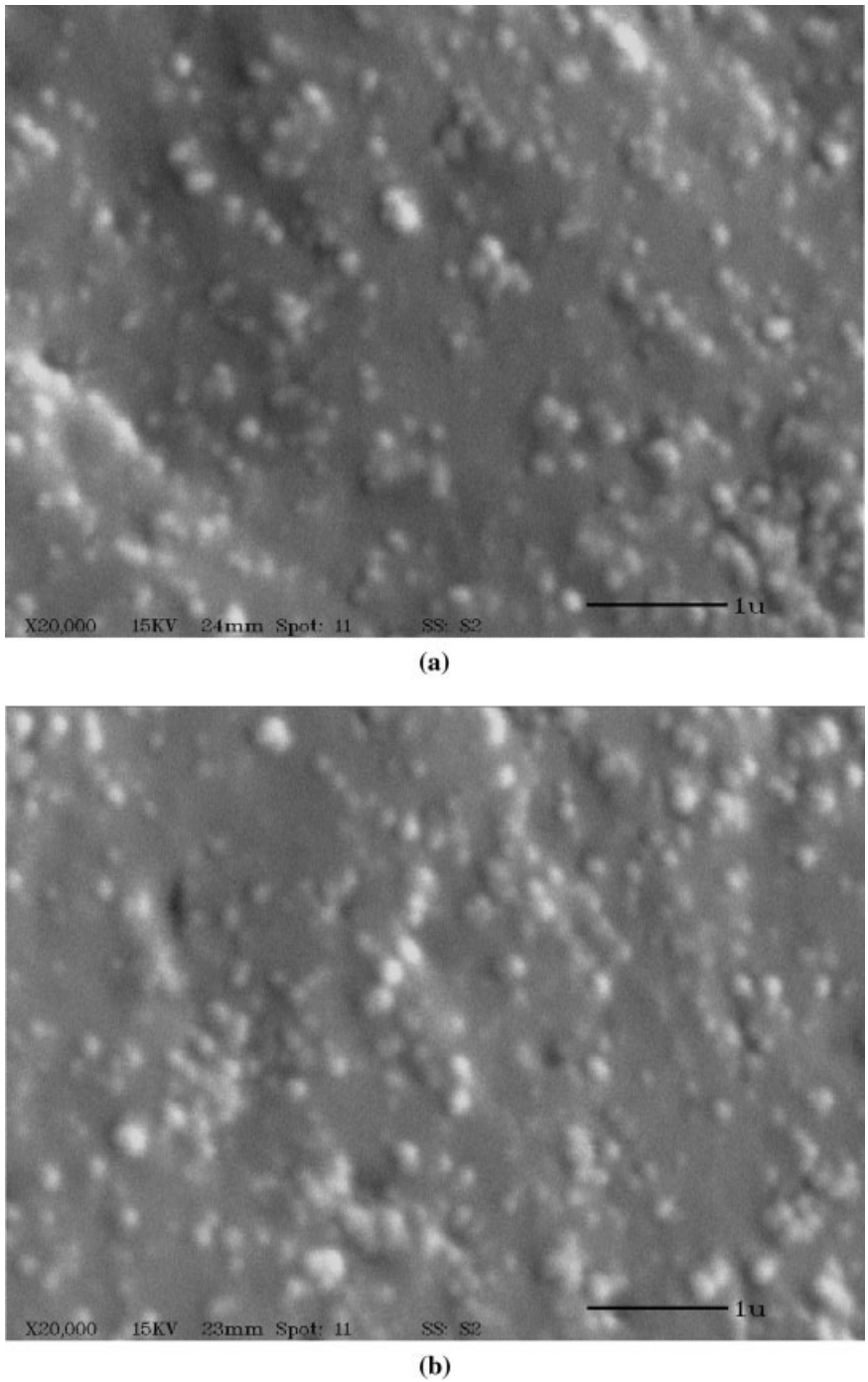


**Figure 3.** Liquid nitrogen fractured surfaces of a CB/SB composite containing 30% CB aggregate. To show the homogeneous distribution of CB, two micrographs were taken from different parts of the same specimen. The scale bar shown is 1 $\mu$m.

is summarized in Figure 5. Above the glass transition region, the addition of 40 wt % of SPI to the styrene–butadiene rubber causes a significant increase (~2.5 decades) of the elastic modulus in the rubber plateau region [Fig. 5(a)]. To study the reinforcement mechanism, the small strain elastic moduli of SPI composites were measured and plotted against volume fractions. The result is shown in Figure 5(b) and a transition of modulus between 6 and 8% volume fraction was observed. This transition is identified as the percolation threshold. Previously, Wu and

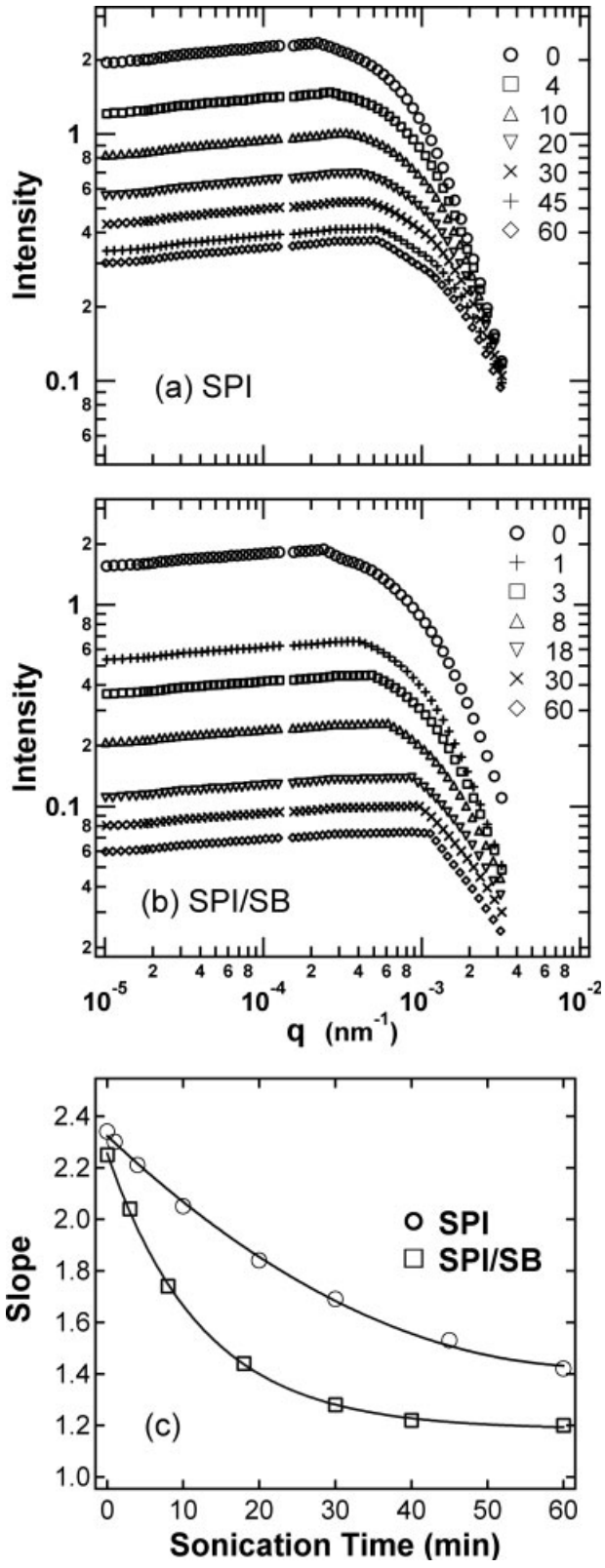


coworkers[29] obtained a ratio of ~7 for the relative storage modulus, $G'_c$(composite)/$G'_p$(matrix), when the rheological measurements were compared with the conductivity measurements in six polymer/carbon filler composites with their percolation threshold varying greatly from 1 to 12 phr (parts per hundred parts of rubber). It is interesting to note that when $G'_p = 0.23$ MPa for SB is multiplied by 7, it gives $G'_c = 1.6$ MPa, which falls within the transition region between 6 and 8 vol % [Fig. 5(b)]. Above the transition region, the best linear fit to the data gives a slope of 2.6, which is smaller compared with other carbon black composites prepared by compression molding method. The CB composites prepared with the same SB matrix in this study showed a similar slope as that of SPI composites. The smaller slope indicates a lower fractal dimension of these SPI and CB aggregates according to the CCA model. This also indicates that the filler aggregate structure is strongly influenced by the method of preparation. The estimation of fractal-like dimension was proposed by Shih and coworkers.[12] For colloidal gels above gelation threshold, the elastic modulus has been related to the fractal structure by the following relation in the strong-link regime.

$$k \sim \phi^{(d+x)/(d-D)} \tag{1}$$

where $K$ is the macroscopic elastic constant, $\phi$ is the overall particle concentration, $d$ is the Euclidean dimension of the system, $x$ is the backbone fractal dimension with a value between 1 and $D$ to provide a connected path, and $D$ is the fractal dimension of the colloidal aggregates. CCA model proposed by Kluppel and Heinrich[11,13,14] for filled elastomers is similar to eq (1). Since the $G'$ of the rubber composites are much greater than the $G'$ of the matrix, the small strain modulus is dominated by the strength of filler network. Therefore, the eq (1) is applicable to the current composites and $D$ is estimated to be 1.3–1.5 from the slope in Figure 5(b). The filler–rubber interaction does not change the

**Figure 4.** (a) Scattering intensity versus scattering vector $q$ for a dilute SPI dispersion. The sonication time in minutes is indicated for each curve. (b) Scattering intensity versus scattering vector $q$ for a dilute SPI/SB dispersion. The sonication time in minutes is indicated for each curve. (c) The change of slopes of the scattering intensities in the limited $q$ region (0.0023–0.0032 nm$^{-1}$).

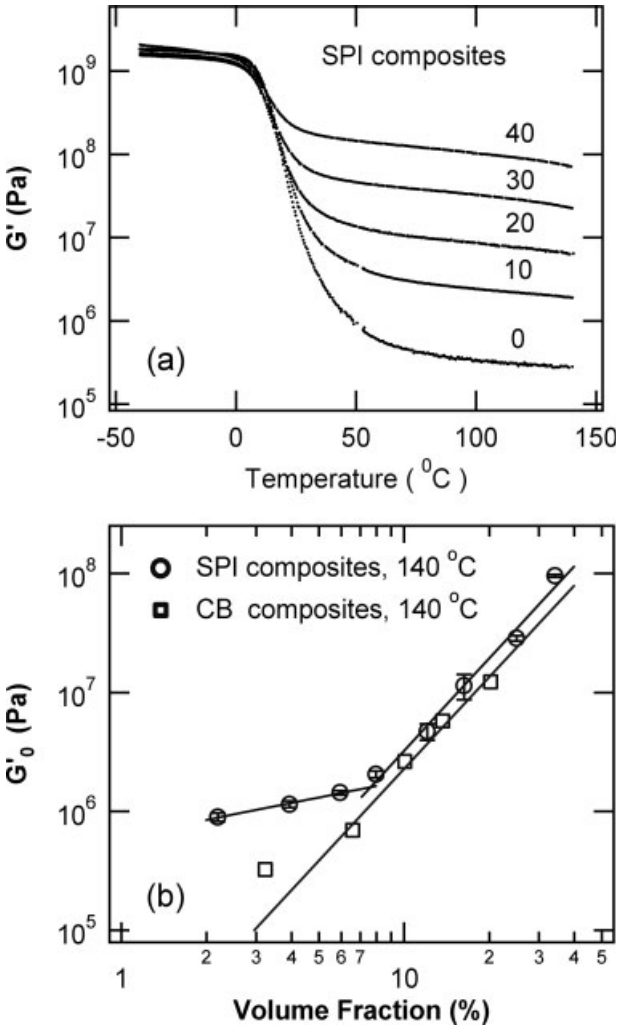


**Figure 5.** (a) Shear elastic moduli of rubber composites with 0–40% of SPI in the temperature range of −40 to 140 °C. (b) Shear elastic modulus versus volume fraction showing a transition between 6 and 8% volume fractions of protein. The straight lines are the best fit to experimental data. The measurements were conducted at 0.16 Hz (1 rad/s) and 0.05% strain.

slope [Fig. 5(b)] significantly because it only increases the effective volume fraction as estimated by the following equation.[11]

$$\varphi \approx \left[\frac{(d+2\Delta)^3 - 6d\Delta^2}{d^3}\right]\phi \qquad (2)$$

Where $\varphi$ is the effective filler volume fraction, $\phi$ is filler volume fraction, $d$ is the particle diameter, and $\Delta$ is the thickness of the immobilized rubber shell on the particle surface. In eq 2, the front factor converting the filler volume fraction to the effective volume fraction is approximately constant for a filler–rubber composite.

### Frequency Dependent Properties

Figure 6 shows the frequency dependent moduli of SPI composites. The reference temperature used to obtain the master curves is set to the glass transition temperature of the SB matrix, 10 °C. As the frequency decreased, the elastic modulus of SPI composites in the low frequency region became less frequency dependent and its value increased as the filler content was increased. This is a typical pseudo solid like behavior in reinforced rubber composites. For a true solid, $G'$ is much greater than $G''$ and both $G'$ and $G''$ are independent of frequency. The frequency shift factors used to construct the master curves is shown in Figure 7. The value of moduli shift factor, $b_T$, for both SPI and CB composites is fluctuating in the range of 1.0 ± 0.2. From 0 to 30% filler concentration, there are little concentration dependence of $a_T$ for both SPI and CB composites. This indicates that the temperature dependence of relaxation behavior is similar in the polymer matrix and filled composites. The 40% SPI filled rubber composite, however, showed a more significant concentration dependent $a_T$. This indicates that the temperature dependence of the relaxation behavior in the 40% SPI composites starts to deviate from the SB matrix. Cole–Cole plot shown in Figure 8 also indicates an obvious single relaxation mode for both filler and rubber matrix. However, there appears to be an emerging second relaxation mode at the lower frequency region adjacent to the first relaxation mode. The extent of emerging second relaxation mode also appears to be proportional to the filler content. The emerging second relaxation mode is likely due to the presence of filler-immobilized rubber phase. The temperature dependence of frequency shift factors can be fitted with Williams–Landell–Ferry (WLF) equation.[30]

$$\log a_T = \frac{-C_1(T - T_g)}{C_2 + T - T_g} \qquad (3)$$

The fitting parameters, $C_1$ and $C_2$, are listed in Table 1. Both parameters follow the same trend to increase as the filler content is increased from 0 to 10% filler, and then decrease as the filler content continues to increase. Different batches of the same SB latex were used in the preparation of SPI and CB composites. Table 1 shows that different batches of SB latex have slightly different $C_1$ and $C_2$. However, the interpretation is not affected by such variation. The comparison of Doolittle equation and WLF

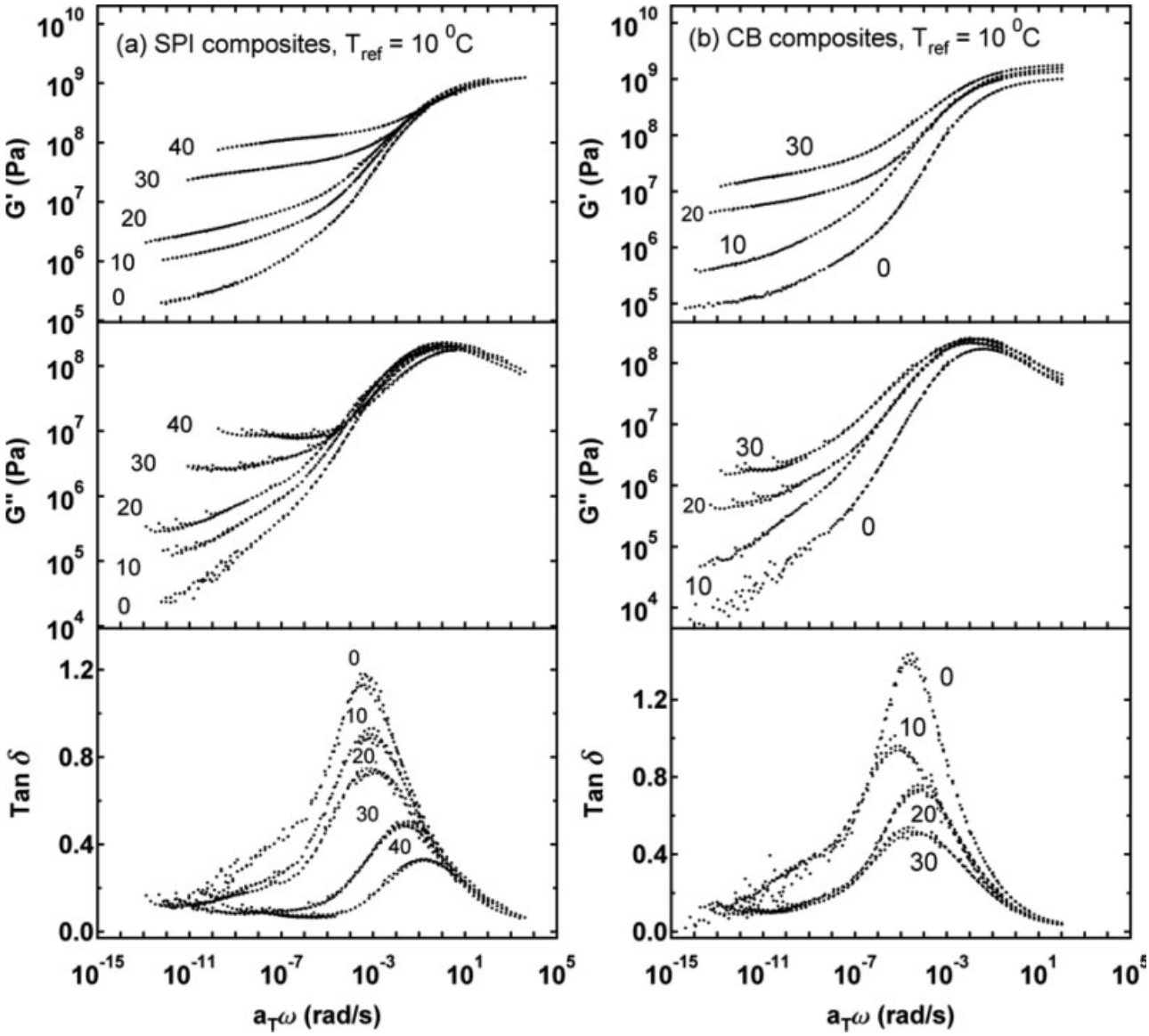


**Figure 6.** Time–Temperature superposition experiments with a reference temperature of 10 °C. (a) SPI concentration in the composites is from 0 to 40% by weight. (b) CB concentration in the composites is from 0 to 30% by weight.

equation[30] allows the estimation of the fractional free volume ($f_g$) at $T_g$ and the coefficient of thermal expansion of the fractional free volume ($\alpha_f$) above $T_g$ from $C_1$ and $C_2$. The semi empirical Doolittle equation for the viscosity ($\eta$) of a liquid is expressed as

$$\ln \eta = \ln A + B\left(\frac{V - V_f}{V_f}\right) \tag{4}$$

where $V$ is the total volume of the system, $V_f$ is the free volume available to the system, and $A$ and $B$ are constants. By assuming that fractional free volume increases linearly with temperature above $T_g$, it can be shown[30] that

$$\log a_T = -\frac{B}{2.303\, f_g}\left(\frac{T - T_g}{(f_g/\alpha_f) + T - T_g}\right) \tag{5}$$

From eqs (3) and (5), $f_g$ and $\alpha_f$ can be estimated by taking $B$ as unity.[30] In Table 1, both $f_g$ and $\alpha_f$ decrease as the filler content is increased from 0 to 10% and then increase as the filler content continues to increase. The trend indicates that the effect of filler–rubber interactions changes

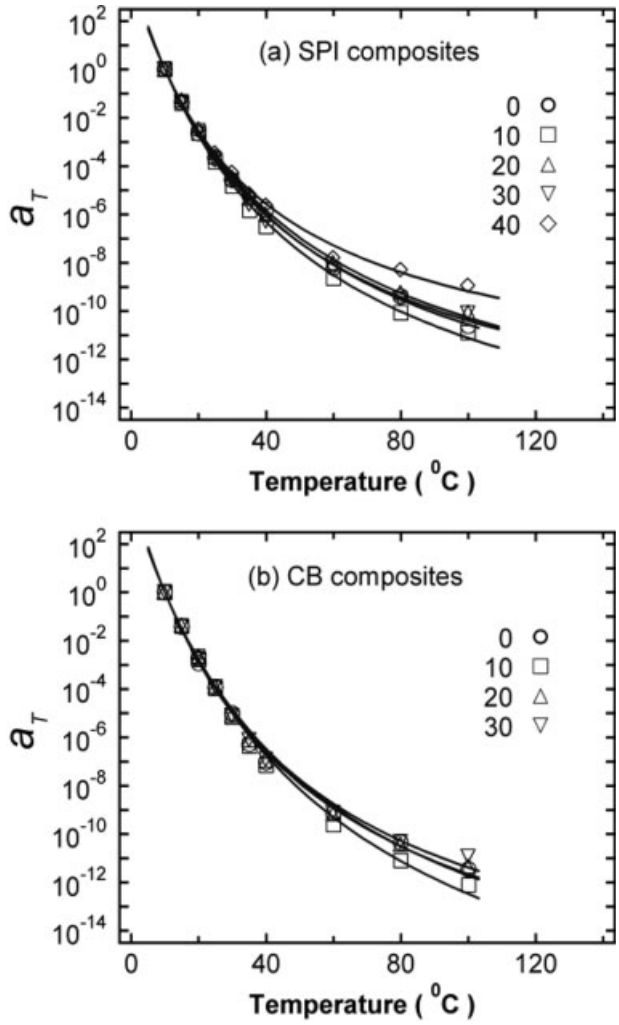


**Figure 7.** Frequency shift factors used to construct Time–Temperature superposition curves for SPI and CB composites. The reference temperature is 10 °C.

the free volume of the rubber matrix and also indicates a transition at ~10 wt % of filler. Compared with Figure 5(b), the transition in the free volume of both SPI and CB composites is approximately corresponding to the transition of the storage modulus near the percolation threshold. SPI composites also appear to have a greater $f_g$ and $\alpha_f$ than the CB composites. This indicates the filler–rubber interactions are different in these two types of composites. The difference can result from (1) different surface areas from different size of filler aggregates (Fig. 2) and (2) different types of interactions. The difference in the surface area alone does not explain the greater fractional free volume in SPI composites because they have smaller filler surface area at the same volume fraction of filler. Therefore, the filler–rubber interaction is an important factor to explain the difference in the fractional free volume between SPI and CB composites.

Figure 6 also shows that the loss modulus at low frequency region increases systematically with filler content. This was explained as the slower relaxation modes at this region are affected by the presence of filler.[31] The matrix immobilization by shorter and shorter space between protein aggregates results in a systematic increase of G″ . On the other hand, the filler does not affect moduli at high frequency region at all. The frequency at G″ maximum is also not affected by the filler loading similar to a previous report on carbon black and other fillers.[31] The glass transition region indicated by tan$\delta$ maximum decreases and shifts systematically to higher frequency as the filler content is increased. This behavior is expected from the crosslinked rubber composites that gradually changed from a soft rubber to a rigid composite as the filler content is increased. The drop in tan$\delta$ at low frequencies is associated with the crosslinked rubber network; the drop at high frequencies is associ-

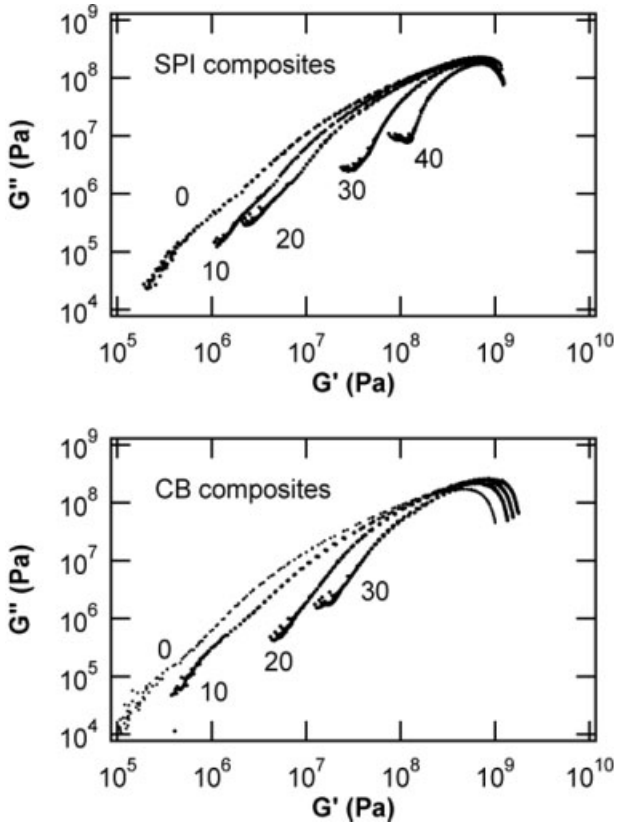


**Figure 8.** Cole–Cole Plots of SPI and CB composites. The reference temperature is 10 °C.

**Table 1.** Fit Parameters of WLF Equation

| Wt % | Vol % | $C_1$ | $C_2$ | $f_g$ ($\times 10^2$) | $\alpha_f$ ($\times 10^4$) |
|---|---|---|---|---|---|
| SPI Composites | | | | | |
| 100% SB[a] | 100% | 17.0 | 55.2 | 2.55 | 4.62 |
| 10% SPI | 8.6% | 18.0 | 55.6 | 2.42 | 4.35 |
| 20% SPI | 17.4% | 16.6 | 55.3 | 2.62 | 4.74 |
| 30% SPI | 26.6% | 16.3 | 50.8 | 2.67 | 5.26 |
| 40% SPI | 36.0% | 13.6 | 43.3 | 3.19 | 7.38 |
| CB Composites | | | | | |
| 100% SB[b] | 100% | 18.8 | 55.5 | 2.30 | 4.15 |
| 10% CB | 6.6% | 21.7 | 66.6 | 2.00 | 3.01 |
| 20% CB | 13.7% | 19.7 | 61.1 | 2.21 | 3.61 |
| 30% CB | 20.2% | 18.2 | 54.3 | 2.38 | 4.39 |

[a,b] Different batches of the same SB latex.

ated with entrance into the glassy zone. The phenomenon was also observed in SB rubber reinforced by polymeric fillers.[31,32] Vieweg and coworkers have studied this transition zone and indicated that the fillers affect the polymer molecular motions with mode lengths of an order of several nanometers.[31]

## Nonlinear Viscoelastic Properties

The frequency and strain dependent moduli of 20 wt % SPI composites are shown in Figure 9. Both rubber and composites are subjected to the eight cycles of dynamic strain at 1 and 15 Hz. The strain cycles have little effect on the rubber matrix [Fig. 9(a)], but have a significant effect on the SPI composites [Fig. 9(b,c)]. The effect is well known as stress softening and is defined as the elastic modulus is reduced after the first cycle of strain. It is observed that a reversible equilibrium is approached only after 4 cycles of strain. The shifting in the loss maximums from the first cycle to the fourth cycle is corresponding to the reduced heat dissipation of broken filler network. The loss maximums were not affected significantly by the increase of frequency and stay at similar strain amplitudes for the strain cycles shown in the Figures 9, 10 and 11. However, the increase of frequency from 1 to 15 Hz in the cyclic strain experiments caused a $G'$ maximum in the low strain region to appear [Fig. 9(c)]. The $G'$ maximum is likely caused by the orientation reinforcement effect from the rearrangement of filler network or filler-immobilized rubber network. It is realized here that a

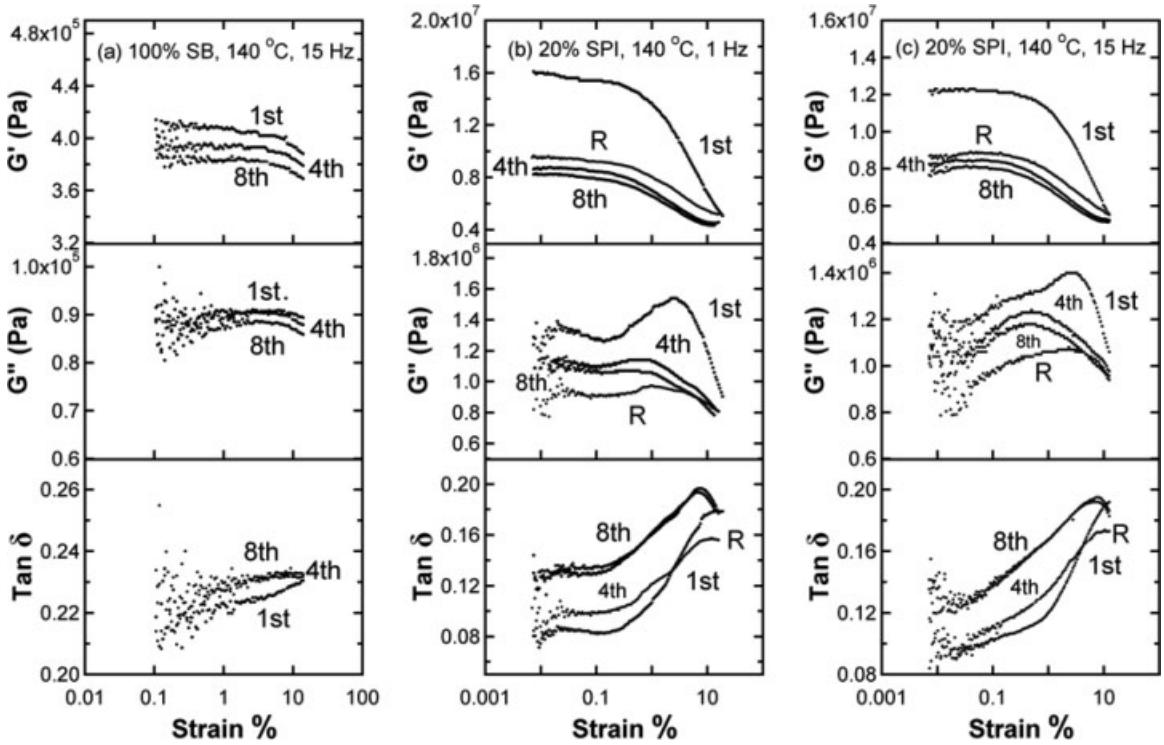


**Figure 9.** (a) 100% SB measured at 140 °C and 15 Hz. (b) 20% SPI measured at 140 °C and 1 Hz. (c) 20% SPI measured at 140 °C and 15 Hz. R indicates the recovery curves.

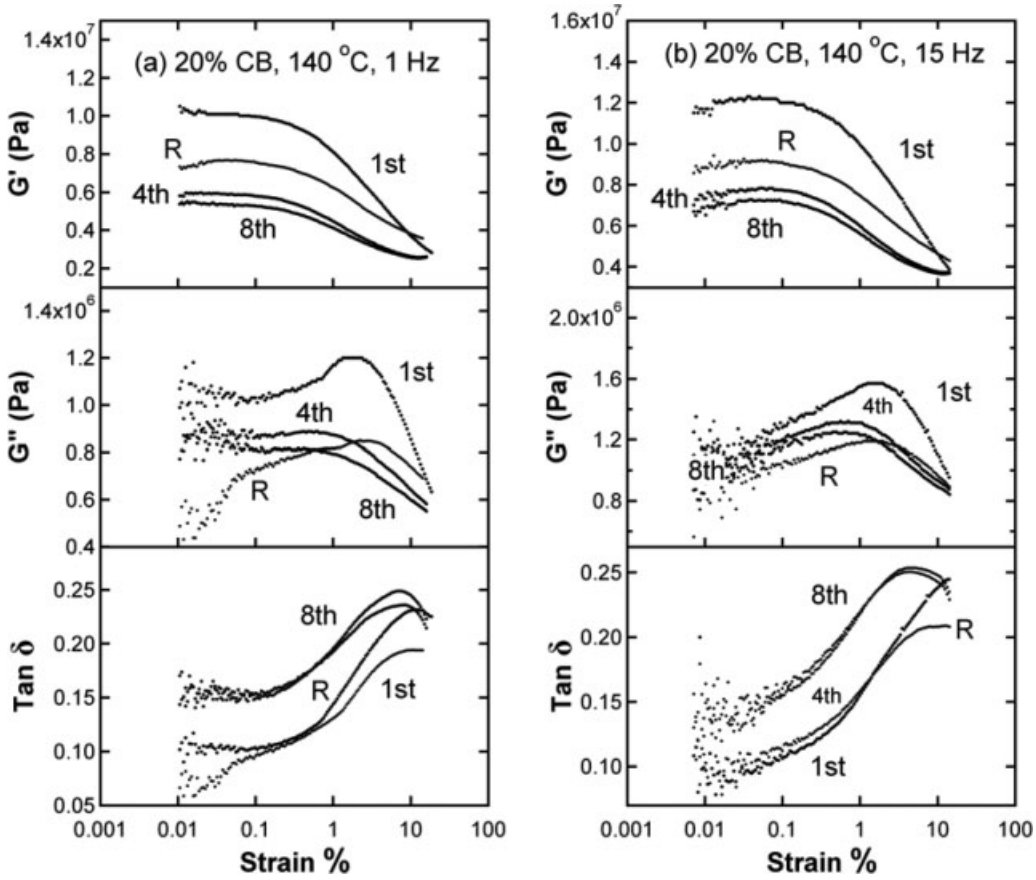


**Figure 10.** (a) 20% CB composite measured at 140 °C and 1 Hz. (b) 20% CB composite measured at 140 °C and 15 Hz. R indicates the recovery curves.

network of immobilized rubber shell on the surface of the filler network is a reflection of the filler network. Such maximum is observed in both SPI and CB composites (Figs. 9–11). It is observed that three factors can cause the $G'$ maximum to become more prominent: (1) the increase in the number of dynamic strain cycles (2) the increase in the amount of fillers (3) the increase of dynamic frequency. As the number of strain cycles is increased, the greater extent of filler network or the immobilized rubber network is broken and the rearrangement of the network can occur by the application of strain. The increase in the amount of filler is equivalent to the formation of a filler network or a filler-immobilized rubber network with a higher crosslinking density. Similar to a highly crosslinked polymer network, more network strands can be broken at a smaller strain amplitude when compared with a network with lower crosslinking density. This can lead to the rearrangement of network structure by a further increase in the strain amplitude. The increase of dynamic frequency produced similar effect by inputting more energy at the smaller strains to break the network. All these factors indicate the $G'$ maximum is related to the breaking and rearranging of the filler network or the filler-immobilized rubber network. Similar observation and explanation were also reported in the literature.[33,34] To further examine the cause of $G'$ maximum, the cyclic strain experiments were conducted on the pure SPI and glassy rubber matrix. It is known that polymer molecules are immobilized on the surface of fillers. To simulate immobilized SB on filler surface, SB was measured at 5 °C, slightly below its glass transition temperature of ~10 °C. The result is shown in Figure 12. It is interesting to note that the rigid SPI showed a reversible structure after four cycles of strain under the measurement conditions. The broken-down structure after four cycles of strain also showed an orientation enhancement type effect in the range of 0.1–0.3% strain as an upturn in $G'$. Both SPI and SB show a $G'$ maximum, but at a different strain. The $G'$ max-

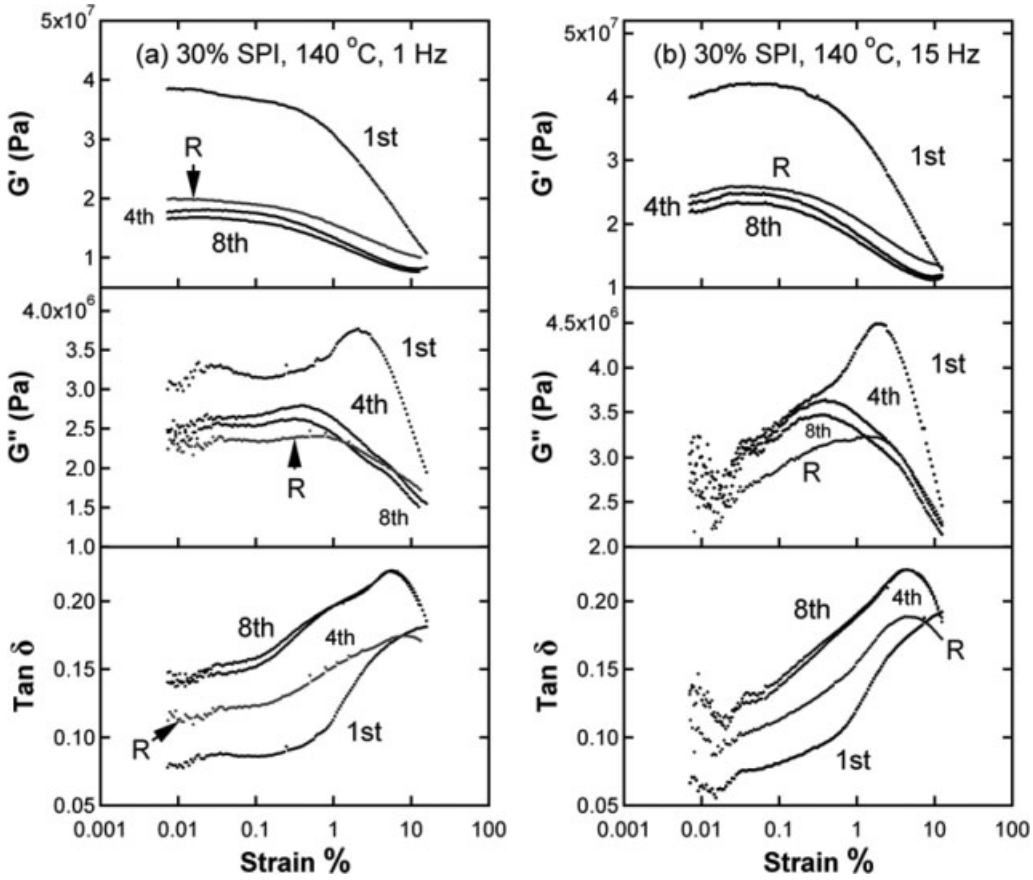


**Figure 11.** (a) 30% SPI composite measured at 140 °C and 1 Hz. (b) 30% SPI composite measured at 140 °C and 15 Hz. R indicates the recovery curves.

imum of SPI occurred at ~0.005% strain, whereas the $G'$ maximum of glassy SB occurred at ~0.03% strain. Compared with the $G'$ maximums in composites (Figs. 9–11), the percent strain at which the $G'$ maximum of glassy SB occurred is closer to that of composites. The observation suggests that the filler-immobilized rubber network, instead of filler network, is responsible for the $G'$ maximums observed in the SPI and CB composites.

The modulus recovery behavior (Figs. 9–11) can also yield some information on the structure of filler network. The recovery behavior is due to the elastic nature of rubber matrix and the competitive attraction between filler–filler and filler–rubber. If there is a stronger attraction between filler and rubber, then it is quite likely that there is more polymer layer between filler aggregates, which leads to a better recovery.[35] On the other hand, a greater filler–filler attraction can lead to a stronger filler network and poorer recovery because there is less polymer layer between filler aggregates. This is similar to the compatibility issue in a two-component polymer blend, where the formation of a nonequilibrium continuous phase from the minor component is determined by the compatibility, among other factors, between two components.[36] The extent of recovery in $G'$ after the composites conditioned at 140 °C for 24 h did not show a significant influence by the increase of measured frequency (Figs. 9–11). This frequency independent feature is consistent with the previous works that the breakup of filler network is only a function of strain amplitude and not affected by the rubber matrix.[34,37] However, CB composites did show a greater extent of modulus recovery in $G'$, likely due to a better filler–rubber interaction. A complete modulus recovery requires the broken-down filler strands in the filler network to return to their original positions before breaking-up, and the reengagement of filler–filler interactions. Previous works on CB reinforced rubber indicated a model of polymer-mediated filler network with a thin layer of polymers between filler aggregates.[34] Such

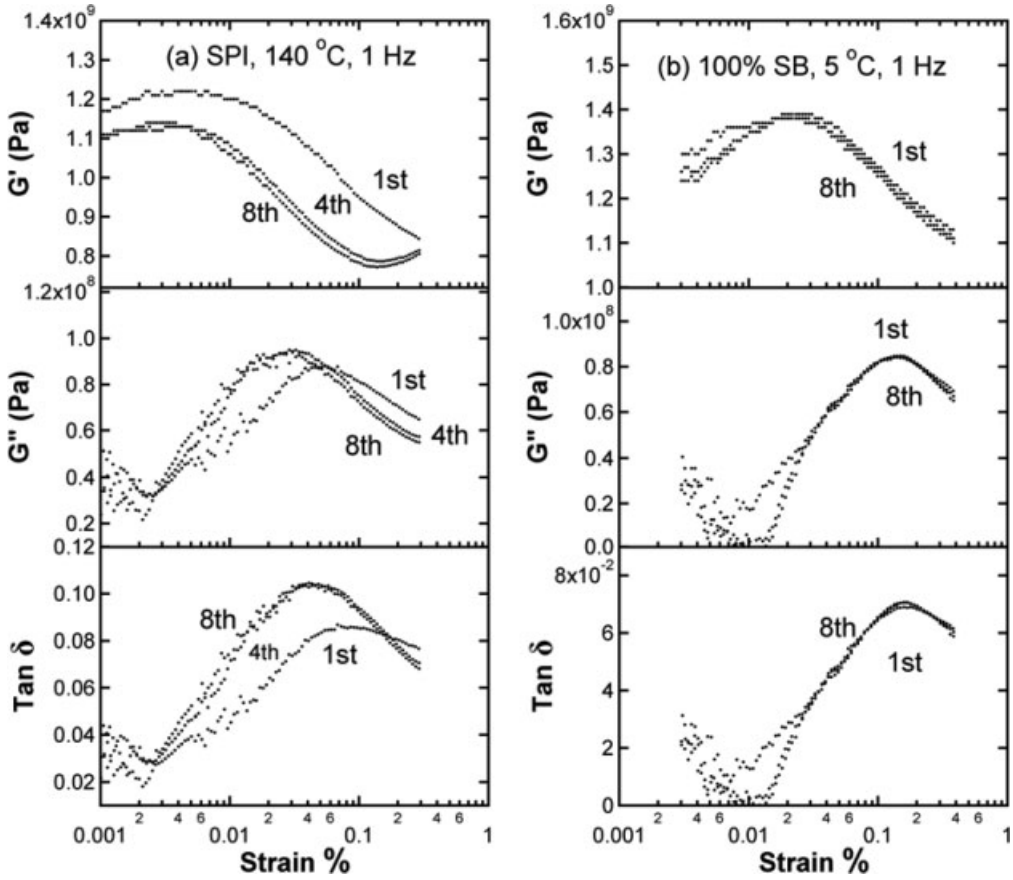


**Figure 12.** (a) 100% SPI measured at 140 °C and 1 Hz. (b) 100% SB measured at 5 °C and 1 Hz.

model can facilitate the recovery, simply because of a more elastic polymer layer between filler aggregates compared with a rigid filler network without a polymer layer between aggregates. This also suggests the higher $G'$ and poorer recovery of SPI composites compared with that of CB composites is most likely caused by the stronger protein network without much polymer mediation between protein aggregates. This explanation is reasonable considering the protein is capable of forming hydrogen and ionic bonds between protein aggregates.

## CONCLUSIONS

The aggregate structure of SPI is consisted of submicron size of globule protein particles as characterized by scanning electron microscopy. The fractal-like aggregates were also characterized by particle size and size distribution. The primary particle size of the SPI aggregates has an average Feret diameter of ~0.33 $\mu$m and a standard deviation of 14%, indicating that the distribution of primary particle size is not monodisperse. The dry size of SPI aggregates is estimated to be ~1.5 $\mu$m. Carbon black aggregates have a number average diameter of ~0.3 $\mu$m. Dynamic shear moduli were measured on the composites filled with different amount of SPI aggregates. About 2.5 decade of increase in the elastic modulus of the composites was observed when the weight fraction of protein was increased to 40%. The composites containing 3–40% by weight of soy protein have a transition in the shear elastic modulus between 6 and 8 vol % of SPI content, indicating a percolation threshold. Compared with CB composites, SPI composites had both a greater fractional free volume and a greater thermal expansion coefficient as estimated from the WLF fit of frequency shift factors, suggesting a different type of filler-rubber interaction. The change of fractional free volume with filler concentration also supports the existence of a percolation threshold. The elastic modulus above the percolation threshold

was used to estimate the fractal dimension of SPI aggregates in the composites. Fractal dimension estimated by the mechanical method is about 1.3–1.5. Nonlinear viscoelastic properties of filler, matrix, and composites were studied by the strain sweep experiments. $G'$ maximums were observed in the composites when the number of strain cycles, filler content, or frequency was increased. This is attributed to the rearrangement and orientation enhancement of filler-immobilized rubber network. The result of nonlinear viscoelastic properties of these rubber composites suggests that the SPI aggregates formed a stronger filler network than the CB aggregates in these composites.

The author thanks Dr. A. R. Thompson for scanning electron microscopy and A. J. Thomas for rheological instrumentation.

## REFERENCES AND NOTES

1. Ismail, H.; Jaffri, R. M.; Rozman, H. D. J Elastomers Plast 2003, 35, 181–192.
2. Nair, K. G.; Dufresne, A. Biomacromolecules 2003, 4, 666–674.
3. Ismail, H.; Shuhelmy, S.; Edyham, M. R. Eur Polym Mater 2001, 38, 39–47.
4. Wang, C.; Carriere, C. J. U.S. Patent 2001, 6,310,136 B1.
5. Wang, S.; Sue, H. J.; Jane, J. J. M. S-Pure Appl Chem 1996, A33, 557–569.
6. Mo, X.; Sun, X. S.; Wang, Y. J Appl Polym Sci 1999, 73, 2595–2602.
7. Wu, Q.; Zhang, L. Ind Eng Chem Res 2001, 40, 1879–1883.
8. Coughlin, E. T. A. U.S. Patent 1936, 2,056,958.
9. Isaacs, M. R. U.S. Patent 1938, 2,127,298.
10. Lehmann, R. L.; Petusseau, B. J.; Pinazzi, C. P. U.S. Patent 1960, 2,931,845.
11. Heinrich, G.; Kluppel, M. Adv Polym Sci 2002, 160, 1–44.
12. Shih, W.; Shih, W. Y.; Kim, S.; Liu, J.; Aksay, I. A. Phys Rev A 1990, 42, 4772–4779.
13. Kluppel, M.; Heinrich, G. Rubber Chem Technol 1995, 68, 623–651.
14. Kluppel, M.; Schuster, R. H.; Heinrich, G. Rubber Chem Technol 1997, 70, 243–255.
15. Garcia, M. C.; Torre, M.; Marina, M. L.; Laborda, F. Crit Rev Food Sci Nutri 1997, 37, 361–391.
16. Richard, J. Polymer 1992, 33, 562–571.
17. Zosel, A.; Ley, G. Macromolecules 1993, 26, 2222–2227.
18. Kan, C. S.; Blackson, J. H. Macromolecules 1996, 29, 6853–6864.
19. Wang, M. J. Rubber Chem Technol 1998, 71, 520–589.
20. Chazeau, L.; Brown, J. D.; Yanyo, L. C.; Sternstein, S. S. Polym Compos 2000, 21, 202–222.
21. Dannenberg, E. M.; Paquin, L.; Gwinnell, H. Carbon black, In Kirk-Othmer Encyclopedia of Chemical Technology, 4th ed.; Howe-Grant, M., Eds.; Wiley: New York, 1992; Vol. 4, pp 1043.
22. Meakin, P. Prog Solid State Chem 1990, 20, 135–233.
23. Meakin, P. Adv Colloid Interface Sci 1988, 28, 249–331.
24. Lin, M. Y.; Klein, R.; Lindsay, H. M.; Weitz, D. A.; Ball, R. C.; Meakin, P. J Colloid Interface Sci 1990, 137, 263–280.
25. Cai, J.; Lu, N.; Sorensen, C. M. J Colloid Interface Sci 1995, 171, 470–473.
26. Sorensen, C. M.; Lu, N.; Cai, J. J Colloid Interface Sci 1995, 174, 456–460.
27. Tence, M.; Chevalier, J. P.; Jullien, R. J Phys 1986, 47 1989–1998.
28. Cai, J.; Lu, N.; Sorensen, C. M. Langmuir 1993, 9, 2861–2867.
29. Wu, G.; Asai, S.; Sumita, M.; Hattori, T.; Higuchi, R.; Washiyama, J. Colloid Polym Sci 2000, 278, 220–228.
30. Aklonis, J. J.; Macknight, W. J. Introduction to Polymer Viscoelasticity, 2nd Ed.; Wiley: New York, 1983; Ch. 3.
31. Vieweg, S.; Unger, R.; Hempel, E.; Donth, E. J Non-Cryst Solids 1998, 235/237, 470–475.
32. Vieweg, S.; Unger, R.; Heinrich, G.; Donth, E. J Appl Polym Sci 1999, 73, 495–503.
33. Newstein, M. C.; Wang, H.; Balsara, N. P.; Lefebvre, A. A.; Shnidman, Y.; Watanabe, H.; Osaki, K.; Shikata, T.; Niwa, H.; Morishima, Y. J Chem Phys 1999, 111, 4827–4838.
34. Yurekli, K.; Krishnamoorti, R.; Tse, M. F.; Mcelrath, K. O.; Tsou, A. H.; Wang, H. C. J Polym Sci Part B: Polym Phys 2001, 39, 256–275.
35. Zhu, A.; Sternstein, S. S. Compos Sci Technol 2003, 63, 1113–1126.
36. Potschke, P.; Paul, D. R. J Macromol Sci Polym Rev 2003, C43, 87–141.
37. Roland, C. M. J Rheol 1992, 36, 1165–1182.